nature structural & molecular biology

Structures of ClpP in complex with acyldepsipeptide antibiotics reveal its activation mechanism

Byung-Gil Lee[1], Eun Young Park[1], Kyung-Eun Lee[2], Hyesung Jeon[2], Kwang Hoon Sung[1], Holger Paulsen[3], Helga Rübsamen-Schaeff[4], Heike Brötz-Oesterhelt[4,5] & Hyun Kyu Song[1]

Clp-family proteins are prototypes for studying the mechanism of ATP-dependent proteases because the proteolytic activity of the ClpP core is tightly regulated by activating Clp-ATPases. Nonetheless, the proteolytic activation mechanism has remained elusive because of the lack of a complex structure. Acyldepsipeptides (ADEPs), a recently discovered class of antibiotics, activate and disregulate ClpP. Here we have elucidated the structural changes underlying the ClpP activation process by ADEPs. We present the structures of *Bacillus subtilis* ClpP alone and in complex with ADEP1 and ADEP2. The structures show the closed-to-open-gate transition of the ClpP N-terminal segments upon activation as well as conformational changes restricted to the upper portion of ClpP. The direction of the conformational movement and the hydrophobic clustering that stabilizes the closed structure are markedly different from those of other ATP-dependent proteases, providing unprecedented insights into the activation of ClpP.

Energy-dependent proteases play a critical role in protein quality control by removing short-lived regulatory proteins as well as misfolded or damaged proteins[1,2]. They usually consist of two components: an energy-consuming ATPase responsible for substrate selection, unfolding and translocation and a proteolytic machine for degradation. Several energy-dependent proteases, such as ClpXP, ClpAP and HslUV in prokaryotes and the 26S proteasome in eukaryotes, share certain general features of the mechanistic process[3]. However, there are substantial differences with regard to substrate recognition, activation, subunit architecture and active-site environment[4]. The ATPase components activate the proteolytic components to enhance catalytic activity, and in turn, the protease components also affect the ATPase activity of activators[5]. Details concerning communication between the two components remain to be elucidated.

The Clp protease system is an energy-dependent protease consisting of ATPases associated with various cellular activities (AAA+), such as ClpX or ClpA in *Escherichia coli* or ClpX, ClpC or ClpE in *B. subtilis*, and the central proteolytic core, ClpP[2,4]. ClpP is a tetradecameric serine protease organized into two stacked heptameric rings that by itself has only limited degradative activity. In general, free ClpP without the related AAA+ components can only degrade small peptides, which enter the secluded proteolytic chamber via small entrance pores. For the degradation of polypeptides and proteins, the ATPases are strictly required; they recognize protein substrates, transport these to ClpP and unfold them in an ATP-dependent process for passage through the pore. The Clp ATPases assemble in hexameric ring structures at the apical surface of ClpP. This protease system is broadly conserved among eubacteria and among chloroplasts and mitochondria of eukaryotic cells (**Supplementary Fig. 1a**) and has been studied extensively[1,2,6–9]. The successful structural analyses of several ClpPs (**Supplementary Table 1**) or ClpP ATPases have given a clear impression of the molecular architecture of the separate components. However, because of the lack of high-resolution structures of any combined high–molecular weight ClpP–Clp ATPase complex, the activation mechanism that depends on the interaction of the two partners remained elusive. The Clp protease system performs important physiological functions such as coordinating cellular differentiation programs or removing protein debris under stress conditions[10]. Disregulation of the Clp protease system can cause severe physiological defects in bacteria and in the case of acyldepsipeptides (ADEPs) can lead to bacterial death, providing a potential avenue for antibiotic development[11,12].

ADEPs belong to the enopeptin class of antibiotics and target Gram-positive bacteria. The parent compound (ADEP1) is a natural product that was improved in a pharmaceutical lead-structure optimization program to yield highly improved synthetic congeners (for example, ADEP2). These improved ADEPs showed impressive antibacterial activity *in vitro*, including against multidrug-resistant bacterial isolates, and therapeutic efficacy in animal models of bacterial infection in the efficacy range of marketed antibiotics[11]. The antibacterial mechanism of ADEPs is based on disregulation of ClpP. Biochemical studies indicate that ADEPs reprogram ClpP, converting it from a highly regulated peptidase that can degrade proteins only with the aid of its partner AAA+ to an independent and unregulated protease[13]. ADEPs prevent formation of the complex between ClpP and Clp ATPases and activate the independent ClpP core to degrade flexible proteins and nascent polypeptides in the course of translation[13].

[1]School of Life Sciences and Biotechnology, Korea University, Seoul, Korea. [2]Biomedical Research Center, Korea Institute of Science and Technology, Seoul, Korea. [3]Department of Chemical Research, Bayer Schering Pharma, Wuppertal, Germany. [4]AiCuris GmbH & Co. KG, Wuppertal, Germany. [5]Present address: Institute for Pharmaceutical Biology, University of Düsseldorf, Düsseldorf, Germany. Correspondence should be addressed to H.K.S. (hksong@korea.ac.kr).

Received 24 September 2009; accepted 8 February 2010; published online 21 March 2010; doi:10.1038/nsmb.1787

To understand the molecular mechanism of this intriguing reprogramming event, we have determined the crystal structures of ClpP from *B. subtilis* (*Bs*ClpP) in the free form and in complex with ADEP1 or ADEP2. These high-resolution structures in combination with structure-based biochemical studies show that ADEPs occupy a position of the ATPase binding site, directly blocking ATPase binding. Furthermore, ADEP binding triggers a reorientation of the ClpP subunits, which disrupts hydrophobic interactions in the N-terminal segment of ClpP, thereby converting the entrance pore from a closed- to an open-gate form. These findings provide insight into the detailed activation step of ClpP and widen our general understanding of the activation mechanism of multimeric cylindrical proteases.

RESULTS

Overall structure of the *Bs*ClpP–ADEP complex

We determined the structures of free *Bs*ClpP (Free1 and Free2) at 2.4- and 3.0-Å resolution in two different crystal forms, and we also determined those of the *Bs*ClpP–ADEP1 (Comp1) and *Bs*ClpP–ADEP2 complexes (Comp2 and Comp3) at 2.0- and 2.6-Å resolution (in two different space groups), respectively (**Table 1**). Each ClpP tetradecamer is in complex with 14 ADEP molecules in a 1:1 stoichiometry, and the antibiotics are located on the apical and distal (top and bottom) surfaces of both *Bs*ClpP heptameric rings in cavities formed by two adjacent ClpP monomers (**Fig. 1** and **Supplementary Fig. 2**). The 14 ADEP binding sites in *Bs*ClpP are deep invaginations in the enzyme surface and contain many hydrophobic residues, including Tyr112, which corresponds to *E. coli* ClpP (*Ec*ClpP) Phe112 (**Supplementary Fig. 1a**). These peripheric pockets were previously proposed in *Ec*ClpP as binding sites for the Ile-Gly-Phe/Lys (IGF/L) loop of *Ec*Clp ATPases ClpX or ClpA (corresponding to ClpX, ClpC and ClpE in *B. subtilis*; **Supplementary Fig. 1b**), which contains (LIV)-G-(FL) residues at the tip[14,15]. We performed a chase experiment to investigate whether ADEPs and ClpX compete for the same binding site. Indeed, an ~2-fold molar excess of ADEP (calculated in relation to ClpP as a monomer) completely blocks the interaction of ClpX with ClpP of both *E. coli* and *B. subtilis* as measured in a functional ClpXP proteolysis assay (**Supplementary Fig. 3**).

ADEP binding triggers entrance-pore enlargement

Previous mutational studies have suggested that the N-terminal segments of ClpP are critical for interaction with Clp ATPases and for accommodating incoming substrates[15–17]. The electron density of the N-terminal segment in free *Bs*ClpP was clear and traceable (**Supplementary Fig. 4a**), although the hairpin loop (residues 8–15) between the first (β1) and second (β0) β-strand could not be built in the current model. Comparison with previous *Ec*ClpP structures[18] reveals that the conformation of the N-terminal segments from free *Bs*ClpP and *Ec*ClpP are essentially similar. Notably, one of several

Table 1 Data collection and refinement statistics (molecular replacement)

	Free		ADEP1 complex	ADEP2 complex	
	Free1	Free2	Comp1	Comp2	Comp3
Data collection					
Space group	*C*2	$P2_12_12$	*C*2	*C*2	*P*1
No. asymmetric unit	7	7	7	7	14
Cell dimensions					
a, *b*, *c* (Å)	121.5, 150.7, 106.54	96.29, 108.12, 152.64	121.65, 151.76, 100.67	121.43, 152.24, 100.38	97.17, 97.24, 100.04
α, *β*, *γ* (°)	90, 121.65, 90	90, 90, 90	90, 120.03, 90	90, 118.98, 90	71.51, 73.89, 77.3
Resolution (Å)	2.4 (2.4–2.49)	3.0 (3.0–3.11)	2.0 (2.0–2.07)	2.6 (2.6–2.69)	2.6 (2.6–2.69)
R_{sym}	6.1 (16.4)	8.2 (49.0)	6.0 (46.7)	9.8 (43.6)	8.4 (30.9)
$I / \sigma I$	33.1 (5.7)	12.8 (1.9)	25.9 (2.6)	12.3 (2.8)	9.6 (2.2)
Completeness (%)	98.6 (90.3)	88.2 (57.2)	98.7 (99.4)	99.3 (98.4)	95.6 (94.6)
Redundancy	3.5 (3.2)	7.5 (5.8)	3.2 (3.0)	3.3 (3.1)	2.0 (2.0)
Refinement					
Resolution (Å)	50–2.4	50–3.0	50–2.0	50–2.6	50–2.6
No. reflections	56,919	26,277	96,696	43,511	86,809
R_{work} / R_{free} (%)	21.5 / 26.5	24.8 / 27.5	21.7 / 25.3	22.6 / 29.5	26.9 / 29.4
No. atoms					
Protein	10,003	9,589	9,289	9,284	18,517
Ligand/ion	–	–	364 (ADEP1) 28 (DMSO) 91 (CHES)	399 (ADEP2) 91 (CHES)	798 (ADEP2)
Water	489	105	667	401	596
B-factors					
Protein	41.6	67.5	37.55	31.6	33.2
Ligand/ion	–	–	49.9 (ADEP1) 52.9 (CHES) 64.9 (DMSO)	40.1(ADEP2) 45.4 (CHES)	42.8(ADEP2)
Water	40.1	43.7	41.01	27.2	22.2
R.m.s. deviations					
Bond lengths (Å)	0.007	0.008	0.006	0.008	0.008
Bond angles (°)	1.15	1.19	1.15	1.22	1.14

One crystal was used for each structure. Values in parentheses are for highest-resolution shell.

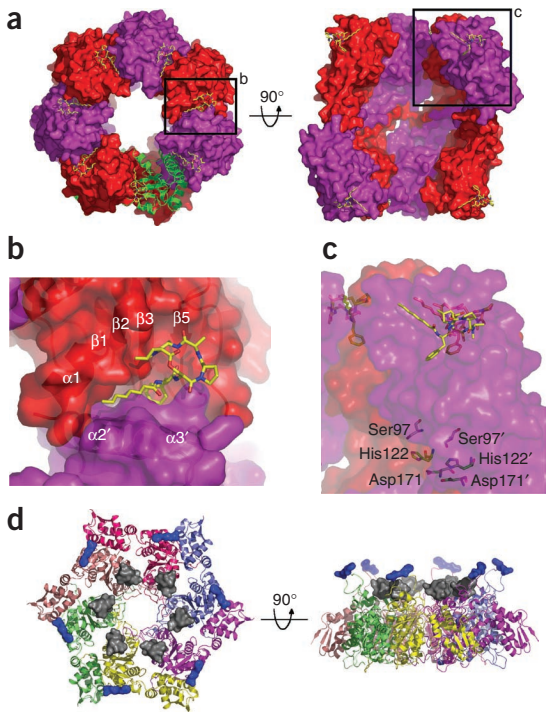

Figure 1 Structure of the *Bs*ClpP–ADEP1 complex and model of the ClpX hexamer. (**a**) Left, the tetradecameric *Bs*ClpP–ADEP1 complex viewed along a sevenfold molecular symmetry axis. Monomers are alternately colored red and magenta, with one monomer shown as green ribbon for clarity. Bound ADEP1 molecules are shown as stick models with carbon, nitrogen and oxygen atoms in yellow, blue and red, respectively. Right, side view of the *Bs*ClpP–ADEP1, displaying the twofold molecular symmetry at the center of the molecule. Three subunits were removed from both the upper and lower heptameric rings to allow a view into the interior of the proteolytic chamber. (**b**) Close-up view of one of the 14 ADEP1 binding sites boxed in **a** (left). The binding site is a complementary pocket composed by two adjacent subunits of ClpP (colored differently). *Bs*ClpP is shown as a ribbon diagram with transparent molecular surface. The secondary structural elements in one subunit and those belonging to the adjacent subunit (marked with a prime symbol (′)) are labeled. (**c**) Close-up view of boxed region in **a** (right), with transparent molecular surface showing the catalytic triads (Ser97, His122 and Asp171) and ADEP1 on the peripheral surface. (**d**) Model of ClpX hexamer (without N-terminal zinc-binding domain) based on the hexameric HslU structure from *E. coli*[31] and the monomeric ClpX structure from *H. pylori*[9]. The two known ClpP binding regions are highlighted as space-filling molecular surface (blue for IGF motifs and gray for pore-2 loops)[25]. Left, view along a sixfold molecular symmetry axis, looking down on the face that interacts with ClpP. Right, a 90° rotation along the horizontal axis yields a side view, showing that the IGF motifs in ClpX represent the most protruding parts toward the ClpP.

reported *Ec*ClpP structures showed alternative conformations for the N-terminal segments[15], suggesting that this region might be flexible. In contrast to the well-resolved N terminus in free *Bs*ClpP, we observed strikingly disordered N-terminal segments in both activator-complexed structures (**Fig. 2a**), implying that ADEP binding might induce additional flexibility in this region. Use of electron microscopy as an additional, independent technology confirmed this result (**Fig. 2b**,**c**). Negative staining and cryo–electron micrographys of free *Bs*ClpP showed a relatively closed entrance pore, whereas the pore was enlarged in the presence of ADEP. The impact of the antibiotics on pore architecture is intriguing, because the ADEP binding sites are located far from the entrance pore—the nearest residues of the ADEP molecule are 11 Å away (**Fig. 1d**).

Structural changes of *Bs*ClpP upon complex formation with ADEP

Superposition of whole *Bs*ClpP tetradecameric ring structures (free versus ADEP1-complexed and free versus ADEP2-complexed) using a secondary-structure matching tool[19] shows an r.m.s. deviation of ~1.2 Å for all chains (**Fig. 3**, **Supplementary Table 2** and **Supplementary Figs. 5** and **6**; more detailed structural comparisons are described in **Supplementary Data**). ADEP binding triggered large movement (>2 Å) of several secondary-structure elements of ClpP located in the ClpX binding side and little movement at the bottom of the ClpP molecules, where the catalytic triads are located (**Fig. 3** and **Supplementary Fig. 5**). These observations suggest that the whole monomer moves as a rigid body within the oligomeric ring structure (**Fig. 3b** and **Supplementary Fig. 5b**). Considering the structurally conserved catalytic triad as a pivot point, the top part of *Bs*ClpP shifted approximately 4° from the axial pore of ClpP, resulting in a slight outward expansion of the heptameric ring. A concerted shift of all ClpP subunits was generated upon complex formation, and many residues of *Bs*ClpP that underwent a shift were not in direct contact with ADEPs (**Fig. 3d** and **Supplementary Fig. 5d**). The regions subjected to relatively large shifts include two α-helices (α1 and α2), four β-strands (β1, β2, β3 and β5) and connecting loop regions. The bottom region of each individual β-strand underwent a minor shift, whereas the upper ADEP binding region shifted markedly. Notably,

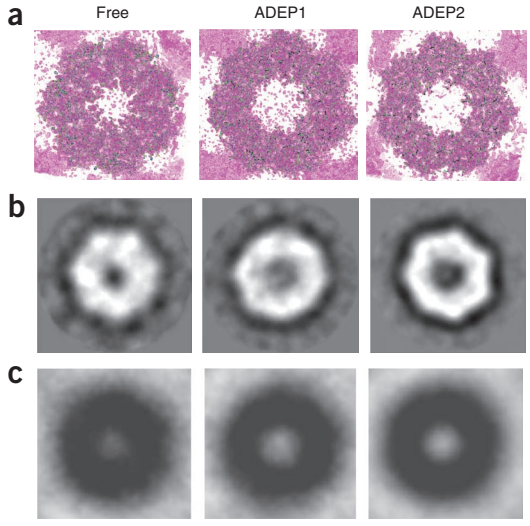

Figure 2 Entrance pore of *Bs*ClpP. (**a**) Top views of the electron density map derived from the structures of free *Bs*ClpP (left), *Bs*ClpP–ADEP1 (middle) and *Bs*ClpP–ADEP2 (right). The $2F_o - F_c$ maps (magenta) were calculated using 30–2.4 Å data for free *Bs*ClpP, 30–2.0 Å for *Bs*ClpP–ADEP1 and 30–2.6 Å for *Bs*ClpP–ADEP2 and are contoured at 1.0σ. The stick models are also presented with the electron density. (**b**) Negatively stained electron microscopic images. Class averages of top views from free *Bs*ClpP (left), *Bs*ClpP–ADEP1 (middle) and *Bs*ClpP–ADEP2 (right). The mean images show seven centers of mass arranged on a ring with low density in the center. The diameters of the whole ClpP ring as measured by the outer rims are ~10 nm in all cases, whereas the central entrance pore changes from ~1.5 nm in free *Bs*ClpP (left) to ~3 nm in *Bs*ClpP–ADEP complexes (middle and right). (**c**) Cryo–electron microscopic images. Class averages of top views from free *Bs*ClpP (left), *Bs*ClpP–ADEP1 (middle) and *Bs*ClpP–ADEP2 (right).

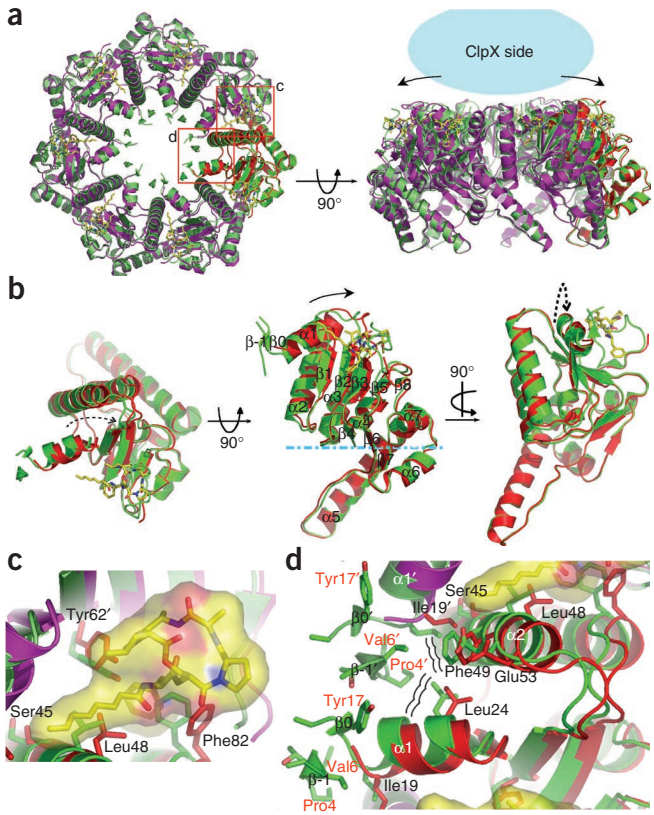

Figure 3 Superposition of free and ADEP1-complexed *Bs*ClpP structures. (**a**) Free (green) and ADEP1-complexed (magenta) structures of *Bs*ClpP, viewed along a sevenfold axis. For clarity, only the upper heptameric ring is shown. The free and complexed monomeric forms are in lighter green and red, respectively. The bound ADEP1 molecules are shown as stick models as in **Figure 1**. Right, a 90° rotation along the horizontal axis showing a side view. The direction of the movement upon complex formation is indicated by the arrows. (**b**) Left, close up of one monomer in the same view as in **a** (left). Middle, a 90° rotation along the horizontal axis. The top portion (above the cyan dashed-dotted line) undergoes a relatively large conformational change in contrast to the lower portion. Right, a 90° rotation along the vertical axis shows no major conformational movement toward neighboring subunits. (**c**) Close-up view of ADEP core-binding region (upper right box in **a**). Bound ADEP1 molecules are represented as stick models with transparent molecular surface. Side chain atoms of mutated ADEP core pocket region residues (L48W, Y62′A, Y62′W, F82A and additional double mutants) of ClpP are labeled in both the free and ADEP1-complexed structures. (**d**) Close-up view of the hydrophobic cluster near the N-terminal β-hairpin region (lower left box in **a**). Side chain atoms of mutated hydrophobic cluster residues near the N-terminal β-hairpin region (I19′S, L24S, F49S and additional mutant E53R) and the disulfide bridge (I19′C and S45C) of ClpP are shown in both the free and ADEP1-complexed structures. The hydrophobic residues (Pro4′, Val6′ and Tyr17) in the N-terminal segment that forms a hydrophobic cluster are also shown and the interaction with a hydrophobic patch in the ClpP core is depicted with wave lines.

structural deviations gradually increased from strand β5 to β1 (from 0.9 to 1.6 Å) in inverse relation to the distance from the ADEP binding site. Moreover, the movement of the two α-helices was much greater than that of the four β-strands. The helices are located further inside than the β-strands and interacted with the N-terminal β-hairpin segment from the neighboring subunit in the free *Bs*ClpP structure (**Fig. 3b** and **Supplementary Fig. 5b**). In short, the structural shifts gradually increased toward the center of the ClpP ring upon ADEP binding, and the N-terminal β-hairpin segments showed a structural transition from an ordered to a disordered state, which subsequently enlarged the axial entrance pore of ClpP.

Interaction between *Bs*ClpP and ADEPs

The structure of ADEP1 consists of three parts: a lactone core containing five proteinogenic and nonproteinogenic residues, a phenylalanine linker region and a hydrophobic tail (**Fig. 4a**). Modifications of ADEP1 to yield ADEP2 comprise replacement of *N*-methylalanine within the pentapeptide ring by pipecolic acid (**Fig. 4b**, bottom left), decoration of the phenyl ring in positions 3 and 5 by two highly electronegative fluorine atoms and replacement of the linear conjugated side chain with a shortened cyclohexane-containing moiety. The phenyl ring of ADEPs recognizes the innermost portion of the ClpP binding cleft, formed by Tyr62, Ile92, Leu114 and Leu189 from one subunit and Phe82′ from the adjacent subunit (for clarity, a prime (′) symbol is used to designate a residue from a different subunit).

The bulky macrolactone core of ADEPs also interacts with hydrophobic residues Ile28, Ile90, Tyr112 and Leu189. Difluorination of the phenyl ring at positions 3 and 5 resulted in a substantial increase in antibacterial activity during lead-structure optimization[12]. Here we find one fluorine atom well accommodated in a polar environment formed by the main-chain carbonyl oxygen of Asp78 and the side chain oxygen atom of Thr79, despite the relatively long distances involved for actual hydrogen bonding interactions (3.81 and 3.82 Å on average, respectively). Notably, the side chain of Ile92 shows a different rotamer that generates sufficient room for the other fluorine atom

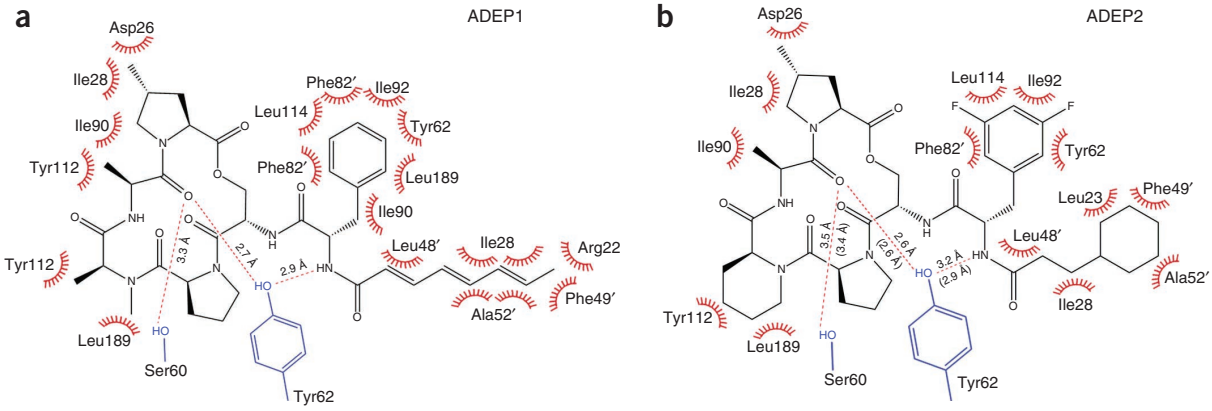

Figure 4 Interaction between ClpP and ADEPs. (**a**,**b**) Schematic diagram showing interactions between *Bs*ClpP and ADEP1 (**a**) and between *Bs*ClpP and ADEP2 (**b**). Residues involved in the hydrophobic interactions are shown as starbursts; hydrogen bonding interactions are denoted by red dotted lines.

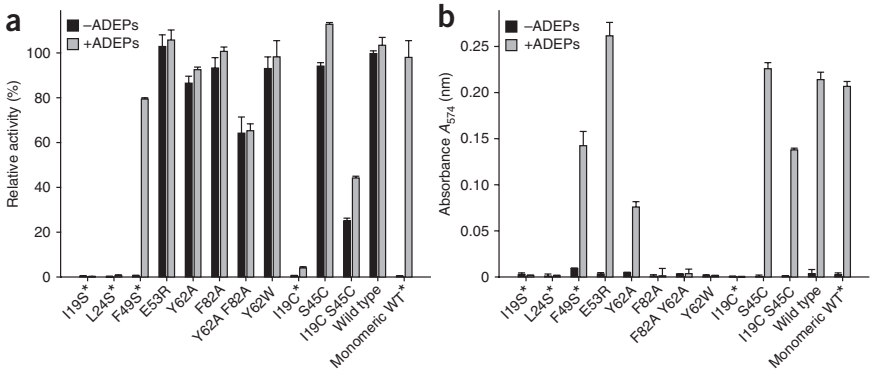

Figure 5 Biochemical results with *Bs*ClpP mutants. (**a**) Peptide hydrolysis activity of wild-type (WT) ClpP and several ClpP mutants from *B. subtilis* in the absence or presence of ADEP. With the exception of the explicitly marked monomeric wild-type *Bs*ClpP, all *Bs*ClpP samples were subjected to gel filtration before this assay (see **Supplementary Fig. 7** for details) to purify the tetradecameric, intrinsically peptidolytic form. Oligomers were successfully isolated in all cases apart form the mutants marked with an asterisk (*), which have an intrinsic oligomerization defect, greatly reducing enzymatic activity. The peptide hydrolysis activity of preoligomerized *Bs*ClpPs remains unchanged in the absence or presence of ADEPs, with the exception of the monomeric F49S* mutant, in which oligomerization and subsequent peptidolytic activity is markedly enhanced by ADEP. Values are normalized to the activity of wild-type ClpP in the absence of ADEP designated as 100% (averages of four or five independent experiments with the indicated s.d.). (**b**) Caseinolytic activity of the same ClpP samples from *B. subtilis* in the absence or presence of ADEP. Mutations in the ADEP core-binding pocket region protect ClpP more from ADEP-mediated disregulation than mutations in the hydrophobic cluster near the N-terminal β-hairpin region.

to face the hydrophobic environment of the pocket. Introduction of fluorine at position 4 of the phenyl ring would have a negative effect on binding due to the limited space, consistent with the loss in antibacterial activity associated with this modification[12].

In contrast to the phenyl ring of ADEPs, approximately half of the bulky closed pentapeptidic core is solvent accessible, and the tail-region interactions are preserved for both ADEPs despite the relatively bulky cyclohexane ring of ADEP2 compared with the linear extended moiety of ADEP1. Residues Arg22 (Leu23 in the case of ADEP2) and Ile28 from one subunit and Leu48′, Phe49′ and Ala52′ from the adjacent subunit accommodate both tail regions (**Fig. 4** and **Supplementary Fig. 4b**,**c**).

Hydrophobic cluster stabilizing N-terminal ClpP segment

Local changes in the ADEP binding site induced a domino effect toward the inner axial pore and triggered the structural transition from a closed- to an open-pore state (**Fig. 2**). When we examined the primary and tertiary structures of the N-terminal β-hairpin segment, we found several hydrophobic residues, such as Pro4′, Val6′ and Tyr17, that formed a hydrophobic cluster with Ile19′, Leu24 and Phe49 (**Fig. 3d** and **Supplementary Fig. 5d**). Two hydrophobic side chains (Pro4′ and Val6′) of the first strand, β1′, interacted with two hydrophobic side chains (Leu24 and Phe49) from helices α1 and α2 from the adjacent subunit. Residue Ile19′ was also involved in this hydrophobic interaction (**Fig. 3d**). The 'up' and 'down' conformations of the N-terminal segment in the crystal structure of a V6A mutant ClpP from *E. coli*[15] suggest a tendency for conformational flexibility due to the decrease in hydrophobicity in this cluster. The hydrophobic nature of Phe17 in the N-terminal segment of *Ec*ClpP (Tyr17 in *Bs*ClpP) may also be critical, as it is known to adopt an alternative conformation[15]. It seems to be crucial for the activation of ClpP that this hydrophobic cluster is formed by two different subunits and is not aligned with the tight intersubunit interface of the so-called 'ClpP body' (excluding the N-terminal segments). This interaction between N-terminal segment and ClpP body might not be strong, which could facilitate conformational transitions involving gate opening and closing. Based on the structural information, we infer that the structural change initiated at the ADEP binding site is transmitted to this hydrophobic cluster region and ultimately weakens the interaction between the ClpP body and N-terminal segment. To confirm this activation mechanism, we performed biochemical investigations.

Oligomerization states and peptidase activity of designed mutants

We placed mutations in prominent ADEP contact sites (Y62A, Y62W, F82A and Y62A F82A) and in the hydrophobic cluster region in contact with the N-terminal β-hairpin (including I19S, L24S and F49S). These residues are well conserved among ClpPs from different organisms (**Supplementary Fig. 1a**). We characterized mutants with regard their oligomeric state, peptide hydrolysis activity and protein degradation potential (**Fig. 5** and **Supplementary Fig. 7**).

It is known from previous studies that *Ec*ClpP possesses peptide hydrolysis activity even in the absence of its physiological activators ClpX or ClpA[20]. This intrinsic activity of *Ec*ClpP, which we observed for our wild-type *Ec*ClpP preparation as well as for mutants, was not further stimulated by the addition of ADEPs (**Supplementary Fig. 8a**). An important prerequisite for this intrinsic peptidolytic activity of *Ec*ClpP is its assembly to a stable tetradecamer[21]. Also, purified *Bs*ClpP tetradecamer, which could be obtained after purification in 10% (w/v) glycerol (**Supplementary Fig. 7a**), was already intrinsically active and did not require ADEP for peptide hydrolysis (**Fig. 5a**). However, *Bs*ClpP in its monomeric form (wild type and mutant), which occurred during preparation in the absence of glycerol, only showed marginal peptidase activity toward succinyl-Leu-Tyr-7-amido-4-methylcoumarin (**Fig. 5a**). ADEPs promoted oligomerization of *Bs*ClpP as they settled in between the subunits to stabilize the oligomeric state of *Bs*ClpP and, consequently, to activate the monomeric ClpP fraction for peptide hydrolysis (**Fig. 5a**). We performed all assays for *Bs*ClpP activity with the appropriate oligomeric forms except for several mutants (I19S, L24S and F49S; marked with a star in **Fig. 5**) that could be obtained as monomers only, despite the presence of glycerol in the preparation buffer, indicating oligomerization defects. Notably, ADEP promoted assembly of the F49S mutant to the tetradecamer (**Supplementary Fig. 7d**), thereby fully restoring its peptidase activity (**Fig. 5a**), whereas the oligomerization defects of I19S and L24S mutants seemed too severe to be counterbalanced by ADEP addition.

Caseinolytic activity of mutant ClpPs

In contrast to peptide hydrolysis, the fully functional tetradecameric ClpPs of *B. subtilis* and *E. coli* lack intrinsic proteolytic activity and are capable of casein degradation, which is performed in the physiological context by the Clp ATPases, only in the presence of activators (**Fig. 5b**

and **Supplementary Fig. 8b**). We also observed marked caseinolytic activity in a situation where ADEPs but no Clp ATPases were present, confirming that ADEPs lead to ClpP activation and disregulation.

As expected, mutating ClpP residues that are involved in prominent interactions with the ADEP core, such as Y62A, Y62W and F82A, markedly decreased the ability of the ADEPs to activate ClpP for casein hydrolysis (**Fig. 5b** and **Supplementary Fig. 8b**). The dynamic residue Tyr62, which establishes two hydrogen bonds between its hydroxyl group and the antibiotics' carbonyl backbone and which rotates 90° upon complex formation, had a substantial role in the interaction between ClpP and activator (**Figs. 3c** and **4**). Notably, deletion of its hydroxyphenyl moiety (in the Y62A mutant) still allowed for residual activator activity (**Fig. 5b**), suggesting that this hydrogen bonding is not critical and that binding of ADEPs to ClpP is mediated predominately through the multitude of hydrophobic interactions. Enlarging the size of the side chain (as in the Y62W mutant), however, completely abolished ADEP activity on ClpP, as did deletion of the phenyl ring of Phe82.

The N-terminal hydrophobic cluster mutations (I19S, L24S and F49S) probably weaken the hydrophobic interaction between the ClpP body and N-terminal β-hairpin segment. In *Bs*ClpP, where oligomerization is less robust than in *Ec*ClpP, these mutations already caused difficulties in heptamer formation and consequently resulted in inactivity, so conclusions about their impact on the activation process cannot be drawn. In *Ec*ClpP, however, where oligomer formation still successfully occurred in the mutants, it is obvious that such transitions involving N-terminal disorder facilitate casein degradation.

Effect of subunit linkage on ClpP activity

The Ile19 mutation to serine or cysteine near the hydrophobic cluster in *Bs*ClpP strongly disturbed oligomerization (**Supplementary Fig. 7e**). In both free and ADEP-complexed *Bs*ClpP structures, residues Ile19 and Ser45′ of two adjacent subunits were in close proximity. Their replacement by cysteine resulted in formation of an intersubunit disulfide bridge (**Supplementary Fig. 9**), and the double mutant I19C S45′C behaved solely as a tetradecamer (**Supplementary Fig. 7e**). Notably, introduction of the second mutation (S45′C) into the inactive mutant I19C recovered substantial levels of activity in all three different enzymatic assays (**Fig. 5** and **Supplementary Figs. 8** and **10**). This result proves that oligomerization deficiency is the reason for inactivity of the N-terminal *Bs*ClpP mutants. More importantly, it supports our structural data concerning the directionality of the structural changes in *Bs*ClpP upon complex formation. The movement of each individual subunit of ClpP associated with its activation is unidirectional toward the periphery of the ClpP ring, which does not substantially change the distance between the two residues Ile19 in helix α1 and Ser45′ in helix α2′ (**Fig. 3** and **Supplementary Fig. 5**). From these results, it is clear that each individual subunit of ClpP moves cooperatively and simultaneously in a unidirectional manner for activation.

Active site of *Bs*ClpP

It has been proposed that substrate binding should coincide with structural rearrangement of the active site for proper ClpP activity[18,22]. Specifically, covalent inhibition or substrate binding was shown in the ClpP structures of *E. coli* and *Helicobacter pylori* to induce an approximate 90° rotation of the hydroxyl group of the active site of Ser97, which positions the nucleophile for optimal catalytic activity. Therefore, we determined whether structural rearrangement occurs upon ADEP binding, though the binding site is approximately 20 Å away from the catalytic serine residue (**Fig. 1d** and **Supplementary Fig. 2d**).

Comparison between free and ADEP-bound *Bs*ClpP did not reveal any marked structural differences near the catalytic site, implying that conformational changes are not relayed from the activator binding site to the active center. Furthermore, comparison of the crystal structure of free *Bs*ClpP with the well-known serine protease trypsin in its apo and substrate-complexed states[23,24] reveals a marked structural overlap between the active sites of both enzymes (**Supplementary Fig. 11b**). As the trypsin active site is already active without further structural rearrangement, it can be assumed that all three residues of the ClpP catalytic triad are also already present in an active, optimal conformation for efficient proton transfer from one residue to another, even in the absence of any substrate (**Supplementary Fig. 11** and **Supplementary Table 3**). This finding is further supported by the observation that peptide hydrolysis by ClpP was not enhanced in the presence of ADEPs (**Fig. 5a** and **Supplementary Fig. 8a**).

DISCUSSION

Two principal options for ClpP activation had been discussed in the literature—a gated-pore mechanism and allosteric activation of the active center—neither one yet proven on the basis of experimental data. An earlier structural study of ClpP in complex with a peptide representing the Ile-Gly-Phe loop region failed to provide the intended information about the activation step, because the peptide acted as substrate rather than as an activator[22]. With the recent discovery of ADEPs as small-molecule activators of ClpP, it is now possible to solve the structure of ClpP in its activated state and to deduce the activation mechanism.

ADEPs are exceptional antibiotics in many respects[11,13]. Not only do they act on ClpP as a heretofore-unknown target, but they inhibit the function of ClpP in a way that goes far beyond simple enzyme inhibition: (i) they trigger assembly of ClpP monomers to an operational tetradecamer, (ii) they inhibit all physiological functions of ClpP by abrogating its interaction with partner Clp-ATPases and (iii) they confer independent proteolytic activities to isolated ClpP. Our structural data showing binding of ADEPs to the hydrophobic pocket at the apical surface of ClpP and extension of their tail toward the N-terminal segment provide a clear explanation for all ADEP-mediated effects. First, the location of ADEPs at the interface of two subunits of ClpP stabilizes the intersubunit interaction. Second, by blocking the binding sites of the IGF loops, the antibiotics prevent complex formation between ClpP and Clp ATPases. Third, by inducing higher flexibility in the N-terminal region of ClpP, ADEPs trigger opening of the gated pore, thus allowing access of larger, unfolded substrates to the proteolytic chamber.

Activation mechanism of ClpP

As described previously, the cylindrical shape of the ClpP molecule combined with its flexible N-terminal segments prevents entry of substrate proteins but allows access of small peptides (**Fig. 6a**). The heptameric ring is maintained mainly by the hydrophobic intersubunit interactions of the ClpP body and the hydrophobic cluster including Pro4′, Val6′, Tyr17, Ile19′, Leu24 and Phe49, which stabilizes the whole N-terminal structure. Our structures of ADEP-activated ClpP and our mutant analyses show that antibiotic binding triggers a concerted movement of all ClpP subunits in a specific direction—namely, a unique lateral shift toward the periphery of the heptameric rings (**Fig. 3b** and **Supplementary Fig. 5b**). This conformational change efficiently perturbs the hydrophobic cluster, which is linked covalently to the ClpP body of one subunit while it interacts hydrophobically with the adjacent subunit. During outwards motion of the ClpP body, the weaker noncovalent interactions might be easily broken, thereby

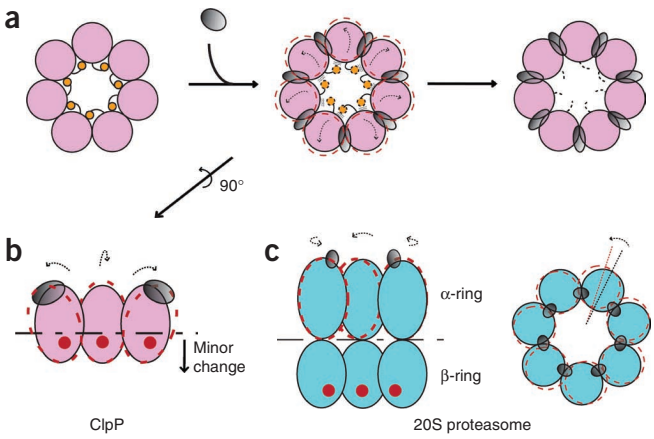

Figure 6 Proposed model for ClpP activation. (**a**) Schematic drawing of ClpP oligomer representing each monomer of ClpP with protein body (large pink circle) linked to the N-terminal segment (small orange circle). For clarity, only the upper heptameric ring is shown. The activator ADEP is depicted as a transparent gray oval. In apo ClpP, the N-terminal β-hairpin segment is stabilized by the hydrophobic patch of the neighboring subunit (left). Activator binding triggers outwards movement of individual subunits of the ClpP body (large circle with red dashed line) as indicated by arrows. This subsequently weakens the interaction between the N-terminal segment and protein body of the neighboring subunit (depicted with wave lines) (middle). Schematic drawing of activator-complexed ClpP (right). (**b**) A 90° rotation of panel **a** along the horizontal axis showing a side view. For clarity, only three subunits at the back of ClpP are depicted. The movement upon complex formation is indicated with red-dashed large ovals and arrows indicate the direction of the movement. The catalytic triads in each subunit are marked with red-filled circles. Below the black dashed-dotted line structural changes upon ClpP activation are limited. (**c**) A similar schematic representation of the eukaryotic 20S proteasome core particle with activator. Only the upper α- and β-rings of the four stacked rings are shown, and only three of the seven subunits are depicted for clarity (left). The movement occurring in the α-ring upon complex formation with activation peptides (derived from the proteasome activating ATPase) is indicated with red-dashed large ovals; arrows indicate the direction of the movement. The active sites located in each β-subunit are marked with red-filled circles, and no conformational changes occur in the β-ring.

destabilizing the whole N-terminal structure and consequently opening the substrate entry pore (**Fig. 6a**). When ClpP interacts with its physiological activators, the primary interaction occurs between the IGF/L loop of ClpX, ClpA or ClpC and the same hydrophobic grooves in ClpP that accommodate the ADEP core. It is reasonable to assume that ADEP serves as a model activator for this specific contact and that the movements observed here will also occur in the presence of the Clp ATPases. According to previous work[25], the interaction of the Clp ATPase's IGF loop is static and stronger than the dynamic pore-2 interaction that the natural activators establish in addition. However, it might well be that binding of the pore-2 loop triggers further movements in ClpP.

Comparison with other ATP-dependent proteases

In multimeric compartmentalized proteases other than the Clp protease, either allosteric activation or a gated-pore process occurs[26–30]. Among the bacterial ATP-dependent proteases, HslVU is the only system to date in which a full multimeric protease complex, consisting of HslV core plus HslU ATPase, has been structurally elucidated[26,31,32]. The structure shows that the entrance pore of HslV widens only slightly upon insertion of the C-terminal ends of HslU into the pockets between the subunits of HslV, but more importantly, the structure also shows that the catalytic threonine reorients in an allosteric activation event[30]. The alternative mechanism, involving a gated process, occurs in the eukaryotic proteasome. The 20S proteasome consists of four stacked heptameric ring structures (α, β, β, α) with the two outer α-rings containing the entrance pores and the two inner β-rings containing the catalytic residues[33–35]. Proteasome activation is proposed to occur through pore opening, as determined by mutagenesis studies of the 20S proteasome core[27,36] and structural analyses of the 20S proteasome with either 11S activator[29,37] or the C-terminal peptide of the proteasomal ATPase[28,38,39].

In the ClpP system the distance between the ADEP binding site and the active sites is over 20 Å, and the catalytic triads do not undergo marked conformational changes upon ADEP complex formation, which speaks against allosteric activation. Instead, the entrance pore of ClpP is enlarged, showing that the N-terminal segments of ClpP act through a gated mechanism analogous to that of the eukaryotic 20S proteasome (**Fig. 6b**,**c**). In the 20S proteasome, activation involves interaction of the α-ring with the activator, which induces structural changes to effect gate opening, whereas no structural changes occur in the β-ring, where the catalytic residues are located. Similarly, the upper half of ClpP, which interacts with ADEP, undergoes a relatively large conformational change, whereas the bottom half of ClpP, where the catalytic triads are located, remains structurally unchanged. Although ClpP consists of only two stacked heptameric ring structures, the underlying operational principle is similar to that of the 20S proteasome.

Details of the activation, however, differ completely between the two systems. Pore opening in the proteasome involves either a stabilization of a specific reverse-turn loop or an ~4° rotation of each α-subunit around Gly128 as the pivot point[39] (**Fig. 6c**; see **Supplementary Data** for varied activation mechanisms of different proteasome activators). Whereas the proteasome undergoes a simple rotation around a pivot point at the nearest residue to the center of the sevenfold axis and a local shift to stabilize the open structure, ClpP activation involves a unique combination of rotation and lateral shift of the whole upper half of each subunit (**Fig. 6a**). The detailed gated mechanism of ClpP activation as outlined here provides a solid framework for understanding the general activation mechanism of multimeric cylindrical proteases.

METHODS

Methods and any associated references are available in the online version of the paper at http://www.nature.com/nsmb/.

Accession codes. Protein Data Bank: Coordinates and structure factors have been deposited with the following accession codes: 3KTG (Free1) and 3KTH (Free2) for free *Bs*ClpP, 3KTI (Comp1) for the *Bs*ClpP–ADEP1 complex and 3KTJ (Comp2) and 3KTK (Comp3) for the *Bs*ClpP–ADEP2 complex.

Note: Supplementary information is available on the Nature Structural & Molecular Biology website.

ACKNOWLEDGMENTS

We thank the staff at 4A beamline, Pohang Accelerator Laboratory, Korea and NW12 beamline, Photon Factory, Japan for help with data collection, B. Hinzen and S. Raddatz (Bayer HealthCare) for the synthesis of ADEPs, M.J. Eck (Dana Farber Cancer Institute) for critical comments on the manuscript and the Advanced Analysis Center in Korea Institute of Science and Technology for providing a

transmission electron microscope. This work was supported by the 21C Frontier Functional Proteomics Project (FPR08B2-270), a Korea Research Foundation Grant (KRF-2007-314-C00176), the World Class University project (R33-10108) and the Plant Signaling Network Research Center. This work was also supported by a Korea Institute of Science and Technology Institutional Grant, by the Systems Biology Infrastructure Establishment Grant provided by Gwangju Institute of Science & Technology to H.J. and by a grant of the Deutsche Forschungsgemeinschaft (FOR854) to H.B.-O. B.-G.L. was supported by a Seoul Science Fellowship and a Korean Student Aid Foundation Science Graduate Research Scholarship.

AUTHOR CONTRIBUTIONS

B.-G.L. and H.K.S. performed X-ray studies; K.-E.L. and H.J. performed electron microscopy studies; B.-G.L. and E.Y.P. performed biochemical studies; K.H.S., H.P. and H.R.-S. performed additional experiments; B.-G.L., H.B.-O. and H.K.S. analyzed data and wrote the manuscript.

COMPETING FINANCIAL INTERESTS

The authors declare no competing financial interests.

Published online at http://www.nature.com/nsmb/.
Reprints and permissions information is available online at http://npg.nature.com/reprintsandpermissions/.

1. Sauer, R.T. *et al.* Sculpting the proteome with AAA+ proteases and disassembly machines. *Cell* **119**, 9–18 (2004).
2. Baker, T.A. & Sauer, R.T. ATP-dependent proteases of bacteria: recognition logic and operating principles. *Trends Biochem. Sci.* **31**, 647–653 (2006).
3. Wickner, S., Maurizi, M.R. & Gottesman, S. Posttranslational quality control: folding, refolding, and degrading proteins. *Science* **286**, 1888–1893 (1999).
4. Gottesman, S. Proteolysis in bacterial regulatory circuits. *Annu. Rev. Cell Dev. Biol.* **19**, 565–587 (2003).
5. Joshi, S.A., Hersch, G.L., Baker, T.A. & Sauer, R.T. Communication between ClpX and ClpP during substrate processing and degradation. *Nat. Struct. Mol. Biol.* **11**, 404–411 (2004).
6. Yu, A.Y. & Houry, W.A. ClpP: a distinctive family of cylindrical energy-dependent serine proteases. *FEBS Lett.* **581**, 3749–3757 (2007).
7. Park, E.Y. & Song, H.K. A degradation signal recognition in prokaryotes. *J. Synchrotron Radiat.* **15**, 246–249 (2008).
8. Kirstein, J., Moliere, N., Dougan, D.A. & Turgay, K. Adapting the machine: adaptor proteins for Hsp100/Clp and AAA+ proteases. *Nat. Rev. Microbiol.* **7**, 589–599 (2009).
9. Kim, D.Y. & Kim, K.K. Crystal structure of ClpX molecular chaperone from *Helicobacter pylori*. *J. Biol. Chem.* **278**, 50664–50670 (2003).
10. Jenal, U. & Hengge-Aronis, R. Regulation by proteolysis in bacterial cells. *Curr. Opin. Microbiol.* **6**, 163–172 (2003).
11. Brotz-Oesterhelt, H. *et al.* Dysregulation of bacterial proteolytic machinery by a new class of antibiotics. *Nat. Med.* **11**, 1082–1087 (2005).
12. Hinzen, B. *et al.* Medicinal chemistry optimization of acyldepsipeptides of the enopeptin class antibiotics. *ChemMedChem* **1**, 689–693 (2006).
13. Kirstein, J. *et al.* The antibiotic ADEP reprogrammes ClpP, switching it from a regulated to an uncontrolled protease. *EMBO Mol. Med.* **1**, 37–49 (2009).
14. Kim, Y.I. *et al.* Molecular determinants of complex formation between Clp/Hsp100 ATPases and the ClpP peptidase. *Nat. Struct. Biol.* **8**, 230–233 (2001).
15. Bewley, M.C., Graziano, V., Griffin, K. & Flanagan, J.M. The asymmetry in the mature amino-terminus of ClpP facilitates a local symmetry match in ClpAP and ClpXP complexes. *J. Struct. Biol.* **153**, 113–128 (2006).
16. Kang, S.G., Maurizi, M.R., Thompson, M., Mueser, T. & Ahvazi, B. Crystallography and mutagenesis point to an essential role for the N-terminus of human mitochondrial ClpP. *J. Struct. Biol.* **148**, 338–352 (2004).
17. Gribun, A. *et al.* The ClpP double ring tetradecameric protease exhibits plastic ring-ring interactions, and the N termini of its subunits form flexible loops that are essential for ClpXP and ClpAP complex formation. *J. Biol. Chem.* **280**, 16185–16196 (2005).
18. Szyk, A. & Maurizi, M.R. Crystal structure at 1.9 Å of *E. coli* ClpP with a peptide covalently bound at the active site. *J. Struct. Biol.* **156**, 165–174 (2006).
19. Krissinel, E. & Henrick, K. Secondary-structure matching (SSM), a new tool for fast protein structure alignment in three dimensions. *Acta Crystallogr. D Biol. Crystallogr.* **60**, 2256–2268 (2004).
20. Thompson, M.W., Singh, S.K. & Maurizi, M.R. Processive degradation of proteins by the ATP-dependent Clp protease from *Escherichia coli*. Requirement for the multiple array of active sites in ClpP but not ATP hydrolysis. *J. Biol. Chem.* **269**, 18209–18215 (1994).
21. Thompson, M.W., Miller, J., Maurizi, M.R. & Kempner, E. Importance of heptameric ring integrity for activity of *Escherichia coli* ClpP. *Eur. J. Biochem.* **258**, 923–928 (1998).
22. Kim, D.Y. & Kim, K.K. The structural basis for the activation and peptide recognition of bacterial ClpP. *J. Mol. Biol.* **379**, 760–771 (2008).
23. Park, E.Y., Kim, J.A., Kim, H.W., Kim, Y.S. & Song, H.K. Crystal structure of the Bowman-Birk inhibitor from barley seeds in ternary complex with porcine trypsin. *J. Mol. Biol.* **343**, 173–186 (2004).
24. Song, H.K. & Suh, S.W. Kunitz-type soybean trypsin inhibitor revisited: refined structure of its complex with porcine trypsin reveals an insight into the interaction between a homologous inhibitor from *Erythrina caffra* and tissue-type plasminogen activator. *J. Mol. Biol.* **275**, 347–363 (1998).
25. Martin, A., Baker, T.A. & Sauer, R.T. Distinct static and dynamic interactions control ATPase-peptidase communication in a AAA+ protease. *Mol. Cell* **27**, 41–52 (2007).
26. Sousa, M.C. *et al.* Crystal and solution structures of an HslUV protease–chaperone complex. *Cell* **103**, 633–643 (2000).
27. Groll, M. *et al.* A gated channel into the proteasome core particle. *Nat. Struct. Biol.* **7**, 1062–1067 (2000).
28. Smith, D.M. *et al.* Docking of the proteasomal ATPases' carboxyl termini in the 20S proteasome's α ring opens the gate for substrate entry. *Mol. Cell* **27**, 731–744 (2007).
29. Forster, A., Masters, E.I., Whitby, F.G., Robinson, H. & Hill, C.P. The 1.9 Å structure of a proteasome-11S activator complex and implications for proteasome-PAN/PA700 interactions. *Mol. Cell* **18**, 589–599 (2005).
30. Sousa, M.C., Kessler, B.M., Overkleeft, H.S. & McKay, D.B. Crystal structure of HslUV complexed with a vinyl sulfone inhibitor: corroboration of a proposed mechanism of allosteric activation of HslV by HslU. *J. Mol. Biol.* **318**, 779–785 (2002).
31. Bochtler, M. *et al.* The structures of HslU and the ATP-dependent protease HslU-HslV. *Nature* **403**, 800–805 (2000).
32. Wang, J. *et al.* Crystal structures of the HslVU peptidase-ATPase complex reveal an ATP-dependent proteolysis mechanism. *Structure* **9**, 177–184 (2001).
33. Bochtler, M., Ditzel, L., Groll, M., Hartmann, C. & Huber, R. The proteasome. *Annu. Rev. Biophys. Biomol. Struct.* **28**, 295–317 (1999).
34. Groll, M. *et al.* Structure of 20S proteasome from yeast at 2.4 Å resolution. *Nature* **386**, 463–471 (1997).
35. Lowe, J. *et al.* Crystal structure of the 20S proteasome from the archaeon *T. acidophilum* at 3.4 A resolution. *Science* **268**, 533–539 (1995).
36. Kohler, A. *et al.* The axial channel of the proteasome core particle is gated by the Rpt2 ATPase and controls both substrate entry and product release. *Mol. Cell* **7**, 1143–1152 (2001).
37. Whitby, F.G. *et al.* Structural basis for the activation of 20S proteasomes by 11S regulators. *Nature* **408**, 115–120 (2000).
38. Smith, D.M. *et al.* ATP binding to PAN or the 26S ATPases causes association with the 20S proteasome, gate opening, and translocation of unfolded proteins. *Mol. Cell* **20**, 687–698 (2005).
39. Rabl, J. *et al.* Mechanism of gate opening in the 20S proteasome by the proteasomal ATPases. *Mol. Cell* **30**, 360–368 (2008).

ONLINE METHODS

Sample preparation. We amplified the *clpP* gene from *B. subtilis* genomic DNA using standard PCR methods. We cloned the product into a pET-26b expression vector with a six-residue histidine affinity tag at the C terminus. We transformed the cloned vector into *E. coli* BL21(DE3) and induced expression of *Bs*ClpP by the addition of 1 mM IPTG at 0.5 OD_{600}. We resuspended harvested cells in buffer A (50 mM Tris-HCl, pH 8.0, 100 mM NaCl, 5% (w/v) glycerol) and then disrupted them by ultrasonication. We clarified the cell lysate by centrifugation and applied it to a nickel–nitrilotriacetic acid column. We further purified eluted fractions by Q-Sepharose anion exchange and Superose 6 gel-filtration chromatography (both from GE Healthcare).

We concentrated purified *Bs*ClpP protein to 10 mg ml^{-1} in buffer A with 1 mM DTT. We dissolved ADEP1 and ADEP2 in DMSO and adjusted the mixtures to a concentration of 80 mM. We prepared *Bs*ClpX according to the procedure above. We prepared EcClpP, EcClpX and GFP-$ssrA^{Ec}$ (GFP-AANDENYALAA) as previously described[40]. We generated EcClpP and *Bs*ClpP mutants and GFP-$ssrA^{Bs}$ (GFP-AGKTNSFNQNVALAA) using a QuikChange kit (Stratagene) and purified them as described above.

Crystallization and data collection. We performed crystallization using the hanging-drop vapor-diffusion method at 22 °C. We prepared the crystallization drops by mixing 2 µl of protein with 2 µl of reservoir solution and then equilibrating the drop against 500 µl of reservoir solution. We obtained two different crystal forms of free *Bs*ClpP. The optimized reservoir conditions for the *C*2 form comprised 100 mM imidazole (pH 8.0) and 0.9~1.1 M sodium citrate. The reservoir solution for the $P2_12_12$ form consisted of 100 mM sodium citrate (pH 5.6), 100 mM Li_2SO_4 and 12% (w/v) polyethylene glycol 4000.

We performed both co-crystallization and soaking to generate crystals of the *Bs*ClpP–ADEP complexes. For soaking ADEPs into pregrown *Bs*ClpP crystals, we applied an ~12-fold molar excess of ADEP1 or ADEP2 solution to free *Bs*ClpP crystals, followed by incubation for ~72–75 h. In contrast to *Bs*ClpP–ADEP1, where soaking experiments were successful (Comp1 in **Table 1**), soaking of ClpP crystals with the less-soluble ADEP2 failed to yield an interpretable electron density map. For cocrystallization, we mixed *Bs*ClpP and ADEP2 in a 1:1 molar ratio and incubated the mixture for 30 min at 4 °C. We crystallized the *Bs*ClpP–ADEP2 complex in two different forms (Comp2 and Comp3 in **Table 1**). We crystallized the whole tetradecameric *Bs*ClpP–ADEP2 complex in the space group *P*1. For the cryo-experiment, we transferred a crystal to reservoir solution containing 25% (w/v) glycerol. We processed the diffraction data with the program HKL2000 (ref. 41).

Structure determination and refinement. We determined the initial *Bs*ClpP structure by the molecular replacement method using the program MOLREP[42]. We obtained the phases using the previously reported structure of EcClpP[15] (PDB 1YG6) as a search model. We mutated the different sequences between *Bs*ClpP and EcClpP using program O[43]. We refined the structure using the program CNS[44]. We maintained a sevenfold noncrystallographic symmetry with tight restraints during the early stages of refinement and relaxed it in the final rounds.

We also obtained phases of *Bs*ClpP–ADEP1 and *Bs*ClpP–ADEP2 by molecular replacement with the program MOLREP[42] using refined *Bs*ClpP structure. We rebuilt the model with program Coot[45] and refined it with CNS[44]. We determined positions of ADEPs using an $F_o - F_c$ difference Fourier map contoured at 2.7σ. We fit the structure of an acyldepsipeptide derivative (number 5, according to ref. 12) into the map and then modified it to ADEP1 or ADEP2 (**Supplementary Fig. 4b**,**c**). We performed refinement of the models as described above. Data collection and refinement statistics are summarized in **Table 1**. We found no Ramachandran outliers in the *Bs*ClpP–ADEP2 structure and only one in the free and ADEP1–*Bs*ClpP structure. For structural analysis, we used Free1, Comp1 and Comp3 structures because Free1 data is of higher resolution than Free2, and we obtained the crystal for Comp3 from different crystallization conditions with cocrystallization method.

Biochemical assays. We quantified proteins by measuring the absorbance at 280 nm or by the Bradford method. We confirmed oligomerization of *Bs*ClpP in solution by gel-filtration chromatography using a Superose 6 column. We pre-equilibrated the column with 25 mM HEPES-KOH (pH 7.6), 200 mM KCl and 10% (w/v) glycerol.

We assayed peptide hydrolysis using the chromogenic peptide succinyl-Leu-Tyr-7-amido-4-methylcoumarin with 0.2 µM ClP_{14}. We used resorufin-labeled casein as a model protein substrate. We measured the proteolytic activity of ClP_{14} (0.15 µM calculated as tetradecamer) in the absence or presence of activators (4.2 µM ADEPs; ~2-fold molar ratio) against 1 mg ml^{-1} resorufin-casein according to the supplier's instructions. For monitoring the proteolytic activity against the folded substrate GFP-ssrA, the assay included 1 µM *Bs*$ClpX_6$ and 2 µM *Bs*ClP_{14} or 0.5 µM *Ec*$ClpX_6$ and 1 µM *Ec*ClP_{14} as well as 2 µM GFP-$ssrA^{Bs}$ or GFP-$ssrA^{Ec}$ in the absence or presence of 0.3 µM ADEP (ADEP1 or ADEP2, but mainly ADEP2). The GFP-ssrA assay buffer contained 25 mM HEPES-KOH (pH 7.6), 200 mM KCl, 5 mM $MgCl_2$, 10% (w/v) glycerol and 0.032% (v/v) Nonidet P-40 in the presence of an ATP regeneration system (0.32 mg ml^{-1} creatine kinase, 16 mM creatine phosphate, 5 mM ATP). We pre-incubated ClpXP (or ClpP–ADEP) for 2 min at 37 °C with all assay components except substrate GFP-ssrA protein. We measured the decrease in fluorescence of GFP-ssrA using a SpectraMax M5 fluorometer (Molecular Devices) at 37 °C (excitation, 467 nm; emission, 511 nm).

Electron microscopy. We diluted purified samples to a concentration of ~0.5–1 mg ml^{-1} for *Bs*ClpP, *Bs*ClpP–ADEP1 and *Bs*ClpP–ADEP2 complexes. We loaded these onto glow-discharged carbon-coated grids and rinsed and stained them with 2% (w/v) uranyl acetate. For cryo-experiments, we loaded samples onto holey carbon film–supported grids and plunge-froze them. We recorded images on a CCD camera (2k, Gatan) using a Tecnai F20 field emission gun electron microscope operated at 200 kV with low-dose mode. We performed image processing and two-dimensional analysis using the EMAN software suite[46]. We selected ~1,500–2,000 particles semiautomatically from individual digital micrographs and also manually sorted them for each sample. We refined these images iteratively using multivariate statistical analysis–based particle classification and averaging. We chose the top views from class averages for each sample.

40. Park, E.Y. *et al*. Structural basis of SspB-tail recognition by the zinc binding domain of ClpX. *J. Mol. Biol.* **367**, 514–526 (2007).
41. Minor, W., Tomchick, D. & Otwinowski, Z. Strategies for macromolecular synchrotron crystallography. *Structure* **8**, R105–R110 (2000).
42. Vagin, A. & Teplyakov, A. An approach to multi-copy search in molecular replacement. *Acta Crystallogr. D Biol. Crystallogr.* **56**, 1622–1624 (2000).
43. Jones, T.A., Zou, J.-Y., Cowan, S.W. & Kjeldgaard, M. Improved methods for binding protein models in electron density maps and the location of errors in these models. *Acta Crystallogr. A* **47**, 110–119 (1991).
44. Brunger, A.T. *et al*. Crystallography & NMR system: A new software suite for macromolecular structure determination. *Acta Crystallogr. D Biol. Crystallogr.* **54**, 905–921 (1998).
45. Emsley, P. & Cowtan, K. Coot: model-building tools for molecular graphics. *Acta Crystallogr. D Biol. Crystallogr.* **60**, 2126–2132 (2004).
46. Ludtke, S.J., Baldwin, P.R. & Chiu, W. EMAN: semiautomated software for high-resolution single-particle reconstructions. *J. Struct. Biol.* **128**, 82–97 (1999).